Pergamon

PII: S0301-9322(96)00009-2

Int. J. Multiphase Flow Vol. 22, No. 4, pp. 685–701, 1996

0301-9322/96 $15.00 + 0.00

MEASUREMENTS OF FLUID/PARTICLE CORRELATED MOTION IN THE FAR FIELD OF AN AXISYMMETRIC JET

F. PREVOST, J. BOREE, H. J. NUGLISCH and G. CHARNAY

Institut de Mécanique des Fluides de Toulouse, ENSEEIHT-INPT-URA CNRS 005, Avenue Camille Soula, 31400 Toulouse, France

(Received 26 October 1995; in revised form 30 January 1996)

Abstract—Typical features of fluid–particle interaction in the far field of an axisymmetric polydispersed particle laden tube jet were measured and analysed in the present study. Measurements up to 45 jet diameters were obtained by using a phase Doppler anemometer. The statistical properties of four particle size classes were obtained in order to cover a wide range of particle relaxation times.

The downstream evolution of the mean longitudinal particle velocity field and of the particle radial and longitudinal turbulent components is first displayed. We show that a Stokes number based on the time scale of the large "structural" eddies is a relevant parameter to describe the selective influence of the jet flow on the particle mean velocity field. The anisotropy between axial and radial fluctuating velocity of the particles is found to increase with increasing particle relaxation time scale.

A method is proposed and validated to determine the statistics of the velocity of the fluid seen by the particles. Measurements are made in the jet far field at $x/D = 30$. Ejection of solid particles in regions of high outward velocity is detected statistically. The fluid–particle correlations are presented and used to analyse the evolution of particle kinetic stresses. The experimental results confirm that the radial particle turbulent velocity is mainly controlled by the dragging by the fluid turbulence and decreases with increasing particle relaxation time compared to the fluid turbulence integral time scale. In contrast, production by the mean particle velocity gradient and transport terms are important mechanisms affecting the streamwise particle turbulence velocity. These mechanisms are responsible for the increase in the streamwise particle turbulence velocity with increasing particle relaxation time. Copyright © 1996 Elsevier Science Ltd.

Key Words: gas–solid flows, particle–turbulence interaction, jet flow, two fluid models, PDA

1. INTRODUCTION

Particle-laden gas flows are extremely important for industrial purposes. They are used for instance in combustion and drying techniques, for cooling purposes and to control dangerous gas clouds by diluting and absorbing. Many experiments have been performed on particle-laden flows and particularly on monodisperse particle-laden jets. We can mention the reference works of Modarress *et al.* (1984); Fleckhaus *et al.* (1987); Tsuji *et al.* (1988); Mostafa & Mongia (1989) and Hardalupas *et al.* (1989) which focused on time-averaged measurements of the mean fluid and particle velocities, mean particle concentration and turbulent components of the two phases.

In parallel to those experimental works considerable efforts have been developed to improve numerical calculations with Lagrangian (Lee & Chung 1987; Berlemont *et al.* 1990) and Eulerian (Elgobashi & Abou-Arab 1983; Picart *et al.* 1986; Simonin 1991) approaches. The application of these statistical approaches to gas–solid turbulent flows shows that the predictions of fluid and particle velocity statistics and consequently of particle dispersion may be strongly dependent on the modelling of the fluid–particle correlated motion, i.e. of the turbulent correlations seen by the particles. As a matter of fact, the undisturbed fluid velocity at the instantaneous spatial location of the particle fixes the instantaneous interfacial transfers of momentum (Deutch & Simonin 1991). Existing validations of the basic assumptions and closure models required for the practical computation of the statistics of the so called "fluid seen by the particles" are presently based on numerical simulations. Simonin *et al.* (1995) have applied large eddy simulation to particle clouds suspended in homogeneous turbulent shear flows to validate their Eulerian approach based on separate transport equations for the components of the kinetic stress tensor and of the fluid–particle velocity covariance.

Another point of view was taken in recent experimental and numerical studies which focused on preferential concentration of particles by turbulence (Eaton & Fessler 1994). The accumulation of dense particles within specific regions of the instantaneous turbulence field was measured mainly by optical methods in experimental flows (Longmire & Eaton 1992, 1994). These studies show that the centrifuging of particles away from vortex cores and the accumulation of particles in convergence zones is characterised by the ratio of the characteristic time of the particles to a characteristic time of the turbulence named the Stokes number (St). A lot of physics can be learn from these studies when one wants, for example, to model the signature of preferential concentration on fluid statistics viewed by the particles. However, as pointed out by Eaton & Fessler (1994), it is frequently quite difficult to select an appropriate turbulent time scale when one deals with complex flows or when a large relative velocity between particles and gas phase is present (Ishima *et al.* 1993). Moreover, if we focus on jet flow studies, the structure of the flow is very difficult to observe in the jet far field and little study has been dedicated to the interaction of the jet far field with particles.

Measurements of fluid–particle interactions in the far field of an axisymmetric polydisperse particle laden tube jet are presented in this paper. The velocity of the 10–50 μm spherical glass particles and the velocity of the fluid are measured simultaneously by a phase Doppler anemometer allowing size and velocity measurements. The statistical properties of four particle size classes (10–15; 20–25; 30–35; and 40–45 μm) are displayed in order to cover a wide range of particle relaxation times. The longitudinal adaptation of the particle motion to the fluid motion is studied in section 3 up to 45 jet diameters. A classical Stokes number based on large eddy time scale is defined. These "structural" eddies (Hunt 1992) are assumed to span the entire jet flow and to represent the dominant structures (Tso & Hussain 1989) in the jet far field. Classical studies of single phase axisymmetric jets show that this time scale increases strongly with axial distance. A wide range of Stokes numbers therefore exists at different locations in the flow.

In the last section, a method is proposed and validated for determining the velocity of the fluid seen by the particles. Accumulation and ejection zones can be detected statistically in the jet far field through the determination of the mean fluid velocity seen by the particles. The longitudinal and radial fluid turbulent Reynolds stresses seen by the particles and the fluid–particles correlations are deduced in order to give further insight into the flow physics and to explain the particular effect of inertia on the degree of anisotropy of the particle fluctuating motion in this free shear flow.

2. EXPERIMENTAL SET UP

2.1. The generation of the particle-laden jet

The set up of the particle-laden jet facility is shown in figure 1. Clean dry air, which passes through a pressure regulator to ensure a constant flow rate ($\pm 1\%$), is seeded by two types of particles: small alcohol particles ($d_p \leqslant 1$ μm) as flow tracers for continuous phase measurements and polydispersed spherical glass beads.

Microscopic visualisations have shown that some batches of spherical particles contain glass fragments. Therefore, all samples were decanted in a rotating bath in order to eliminate these fragments. Figure 2 indicates alcohol and glass particle diameter distributions at the pipe exit obtained by phase Doppler measurements after decantation. The median volume diameter of the glass beads at the pipe exit is about 36.2 μm. Sixty per cent of the total number of particles have diameters between 10 and 50 μm. In order to avoid agglomeration of particles due to humidity, all samples of glass beads were dried in an oven before use. All parts of the experimental setup were grounded in order to minimize the electrostatic effects on the glass particles.

To isolate the effects of flow structures on the glass particles, the experiments were performed at a low particle mass loading ratio M (mass flow of particles divided by air mass flow) close to 8%. Comparison between the continuous phase evolution of the single and two-phase jets for those experimental conditions have shown only a very small influence of the presence of particles on the development of the jet (Prévost 1994). The volume ratio corresponding to this mass loading is about 0.004%. It is much below 0.3%. Particle–particle interactions are thus negligible (Hardalupas *et al.* 1989).

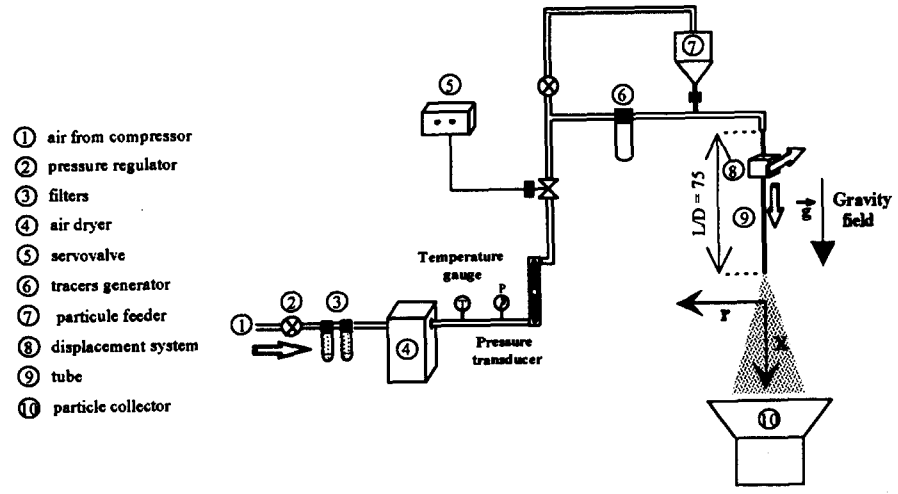

Figure 1. Experimental set up.

The experimental flow configuration is seen in figure 1. The streamwise direction is the x-axis and the radial direction is the r-axis. The vertical jet flow discharges in still ambient air through a glass tube with a length to diameter ratio of 75 ensuring the establishment of a fully-developed profile. The exit Reynolds number based on the tube diameter ($D = 0.01$ m) is 13 100 corresponding to a mean exit velocity of 20 m/s. The exit pipe is mounted on a two axis displacement table driven by a personal computer. The tube is aligned by a cathetometer with a precision greater than 0.1 mm. The table allows measurements in the axial flow direction from the exit to 50 jet diameters with a minimum displacement step of 0.1 mm.

2.2. Measurement facility and acquisition system

A phase Doppler technique (P. D. A. Dantec) is used to measure the mean and fluctuating velocities and the diameter of the spherical particles detected. The optical system is composed of an Argon laser (1.5 W on the green wavelength), a Bragg cell and a lens of 750 mm focal length. A beam expander is required in order to minimise the dimensions of the measurement volume. The resulting beam intersection volume is 1.17 mm long with a diameter of 0.096 mm and a fringe spacing of 2.95 μm. The receiving optics were placed at 41° to the forward scatter direction to minimise the contribution of the reflected light. The signal is processed by a correlator and all data

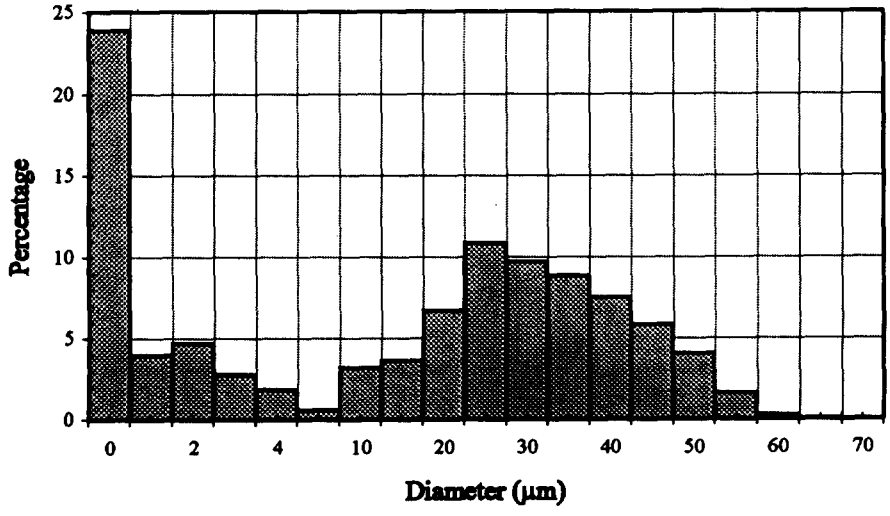

Figure 2. Tracers and glass particles size distribution.

are collected in a personal computer. The software parameters for the size analysis are chosen for the glass beads which does not affect the discrimination between the tracers and the glass beads. The analysis of the behaviour of the polydispersion of glass particles is carried out by dividing the particles into four size classes: 10–15, 20–25, 30–35 and 40–45 μm. The gas phase velocity is obtained by averaging the velocity measurements in the size-class 0–1 μm, composed of alcohol droplets. Despite the lack of accuracy of diameter measurements of particles smaller than few microns with the phase Doppler technique, it has been verified that all the particles in this size-class can be considered as good tracers of the continuous phase. A correction by residence time of the particles in the measuring volume is used to reduce the velocity bias present in velocity measurements (Petrie *et al.* 1988). Measurements of longitudinal or radial velocities are carried out for the continuous and dispersed phases simultaneously. We perform ensemble averaging of at least one thousand independent samples in each size-class. Consequently, estimated statistical relative errors for mean and standard deviation values on the jet axis are, respectively, 2 and 5% with a 95% confidence level.

3. LONGITUDINAL ADAPTATION OF THE MEAN AND FLUCTUATING PARTICLE MOTION

3.1. Characteristic time scales

The jet will be described henceforth using a cylindrical coordinate system (x, r, θ) to indicate the axial, radial and azimuthal directions of the jet. The components of the mean and fluctuating velocity field are denoted, respectively, by (U, V, W) and (u, v, w) where V is the radial component and W is the azimuthal component. No swirling motion was detected ($W \approx 0$) to within our measurement precision. Subscript "0" indicates the exit properties and subscript "c" indicates the centreline properties. Subscripts "f" and "p" indicate, respectively, fluid and particles properties. The symbol $\langle\rangle_f$ and $\langle\rangle_p$ indicates averaging operators associated, respectively, to fluid and particle phases. The expressions u' and v' stand, respectively, for the standard deviation $\langle u^2\rangle^{1/2}$ and $\langle v^2\rangle^{1/2}$.

The Stokes number of a particle size class is defined as the ratio of the particle aerodynamic time constant τ_p to an appropriate turbulent time scale τ_j. The Stokesian particle relaxation time was chosen for $\rho_p \gg \rho_f$:

$$\tau_p = \frac{\rho_p d_p^2}{18\,\mu} \qquad [1]$$

where d_p is the median diameter of the particle size class, ρ_p is the particle density and μ is the fluid viscosity. While the assumption of Stokes flow around the particle is not satisfied for many cases

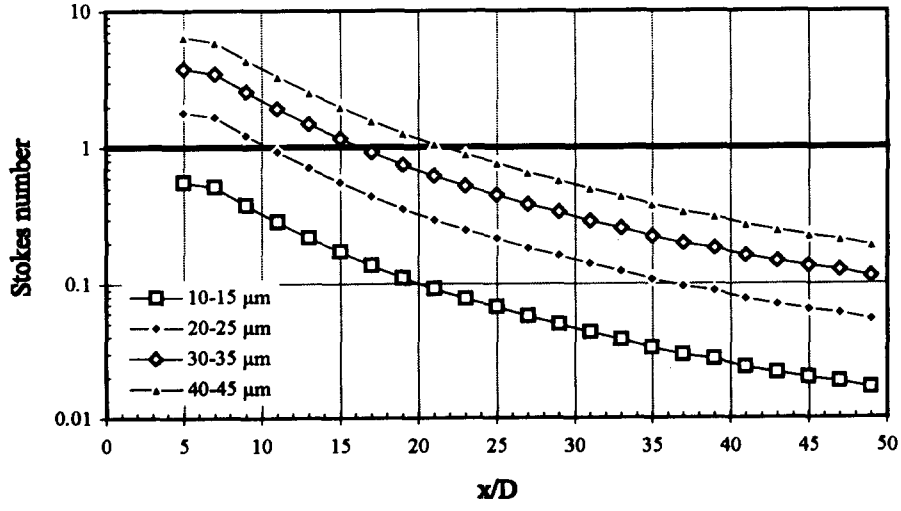

Figure 3. Longitudinal evolution of the Stokes number of the different particle size classes.

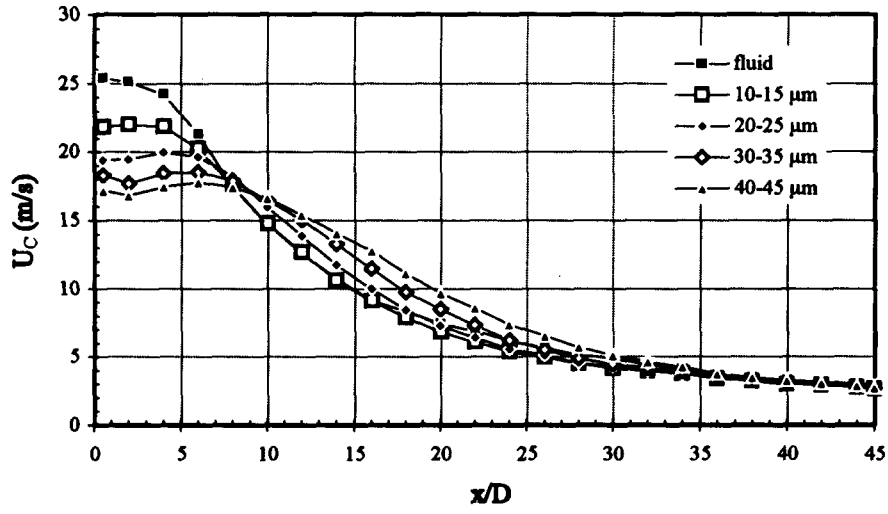

Figure 4. Axial evolution of the fluid and particles mean longitudinal velocity.

in our experimental conditions, this characteristic time calculation remains interesting for particle Reynolds number up to order of unity.

Following Longmire & Eaton (1992), the local particle dispersion seems to be governed mainly by the large-scale turbulent structures of the gas phase. Therefore, the characteristic time of the jet τ_j is chosen as the ratio of a large eddy length scale L to the standard deviation of the fluctuating velocity on the jet axis $u'_{f,c}$. As a first approximation and beyond $x/D = 10$, we take for L the half width of the jet $L = 0.1x$ (Dimotakis *et al.* 1983):

$$\tau_j = \frac{0.1x}{u'_{f,c}}. \qquad [2]$$

It must be noted here that τ_j increases longitudinally as x^2 in an axisymmetric jet.

It is very important to note that this definition of St assumes that the particles have no significant mean velocity relative to the turbulent eddies. Ishima *et al.* (1993) showed that a modified eddy characteristic time taking account of the particle residence time has to be defined to describe particle dispersion in a two dimensional mixing layer with a large relative velocity between particle and gas phase.

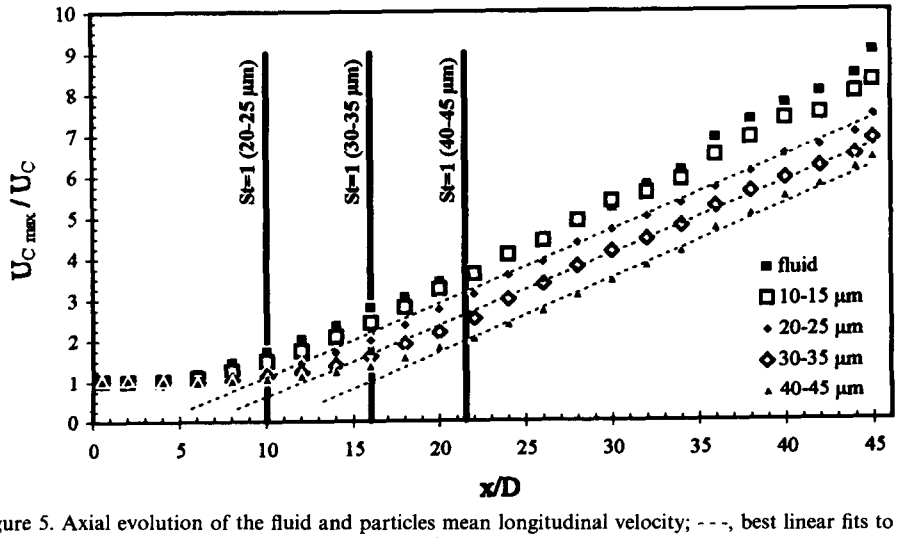

Figure 5. Axial evolution of the fluid and particles mean longitudinal velocity; - - -, best linear fits to the data.

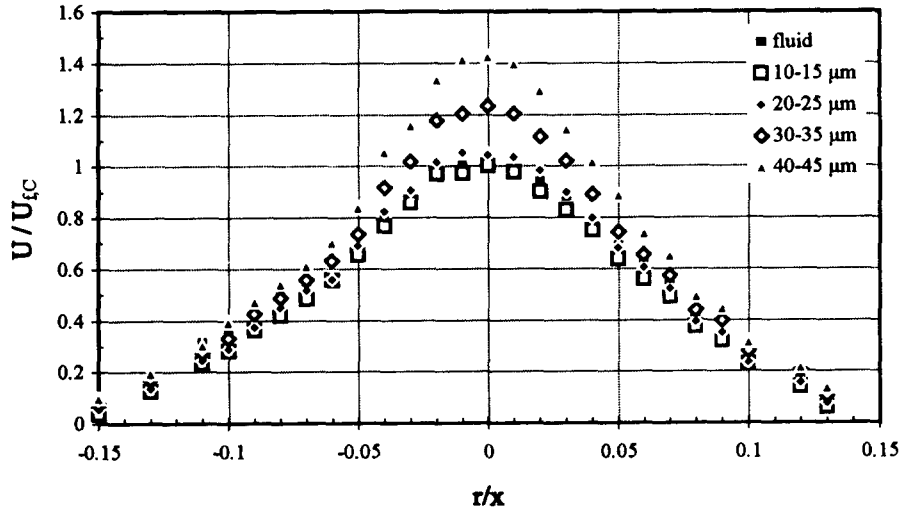

Figure 6. Mean longitudinal fluid and particles velocity profiles at $x/D = 20$.

A Stokes number of order one separates particles following all the fluctuations of the fluid ($St \ll 1$) and particles not following any fluctuation ($St \gg 1$). We have reported in figure 3 the longitudinal evolution of the Stokes number of each size-class of particles studied. We notice the large range of Stokes numbers that exists for our conditions. Moreover, the noticeable longitudinal decrease of St gives us the opportunity to observe changes of behaviour of the different size classes of particles in the region studied (Prévost *et al.* 1994).

3.2. Distribution of the particle mean velocity

The evolution of the axial mean longitudinal velocity for the continuous and dispersed phases is presented in figure 4. We can observe a noticeable relative velocity between the gas phase and the different size-classes of the particles at the jet exit. This phenomenon was already observed before (Hardalupas *et al.* 1989; Heitor & Moreira 1994). It is due to the flow–particle interaction in the tube and to the presence of rebounds of particles along the wall of the tube (Hardalupas *et al.* 1989; Zoltani & Bicen 1991). Planar visualisations at the exit of the tube by a thin laser sheet have supported this hypothesis. In this way, both particles originating from regions of low velocity (next to the tube wall) and particles originating from regions of larger velocity (on the axis of the

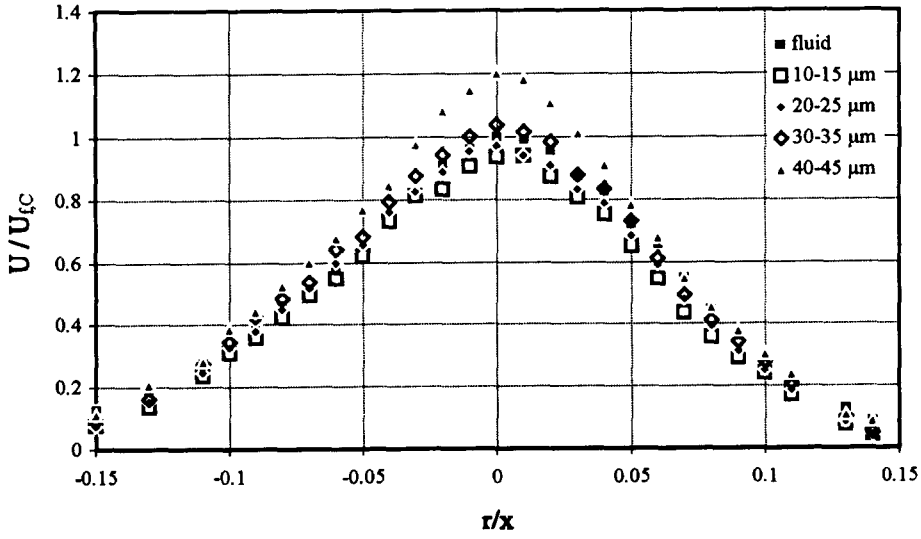

Figure 7. Mean longitudinal fluid and particles velocity profiles at $x/D = 30$.

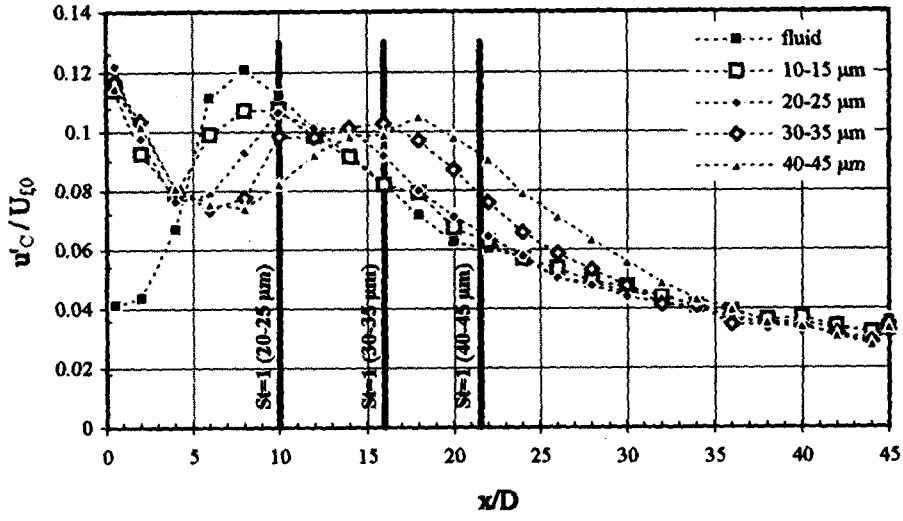

Figure 8. Axial evolution of the fluid and particles streamwise fluctuating velocity.

stream) are flowing by one point in the stream at the exit of the tube. In an Eulerian description, these different contributions tend to decrease the mean particle velocity and to enhance the fluctuating components (see figure 8) close to the exit of the tube. The complete set of mean and fluctuating fluid and particle velocity profiles at the jet exit can be found in Prévost (1994).

Due to this relative motion near the exit, the particles are accelerated by the gas along the nine first diameters until they reach the mean gas velocity. At this point, the mean gas velocity is decreasing with x. Further downstream, all but the smallest particles again lag the fluid behaviour so that their axial velocities decrease more slowly. Thus, the mean particle velocity is larger than the mean gas velocity. At around 40 diameters downstream, the velocity of all classes tends to approach the velocity of the gas phase. The final relative velocity should be, for each class of particles, the very weak free fall velocity of the particles in the stream.

In figure 5, the axial variation of streamwise mean centreline velocity is normalised by the maximum mean velocity measured for each size-class. We see in this figure that after a phase of slow evolution, the slope of the particle mean velocity tends toward that of the gas phase. Moreover, the axial location where the change in the behaviour of the particles of each size-class occurs corresponds to a value of the Stokes number of these size-classes of order one (reported

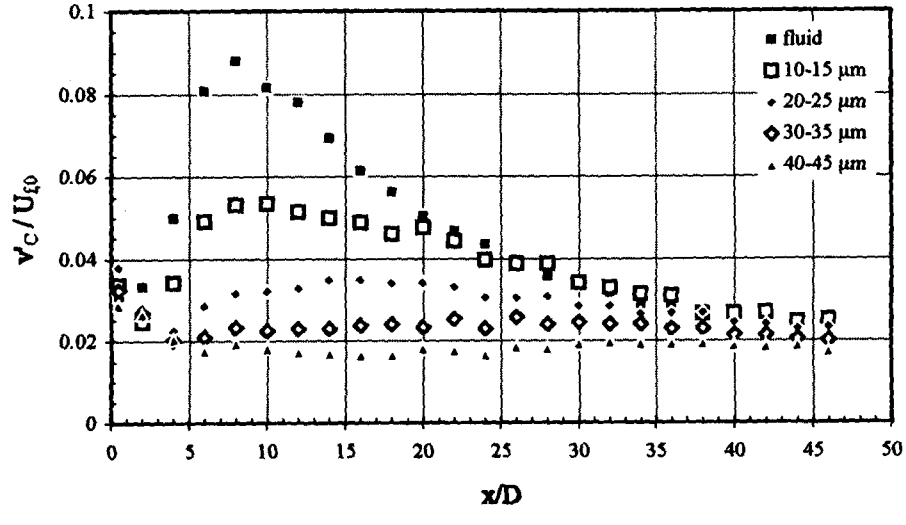

Figure 9. Axial evolution of the fluid and particles radial fluctuating velocity.

in the figure). A virtual origin can be deduced for each size-class at the crossing point of each linear regression curve and of the abscissa axis. The location of this virtual origin is shifted downstream as the relaxation time of the particles increases and, in the jet far field, the influence of the particles relaxation time seems to be embodied in this virtual origin. Prévost *et al.* (1995) found a linear dependance between this location $x_{0,p}$ and the axial position where the Stokes number of the particle size class is equal to one $x_{1,p}$ given by $\tau_j(x_{1,p}) = \tau_p$:

$$\frac{x_{0,p}}{D} = a\left(\frac{x_{1,p}}{D}\right) + b \quad \text{where } a = 0.61 \text{ and } b = -2.17. \qquad [3]$$

The selective influence of the jet flow on the particle size class noticed on the axial evolution is also detected in the transverse profiles. We have reported in figures 6 and 7 the mean longitudinal velocity profiles at 20 and 30 diameters from the exit, respectively, normalised by the mean centreline velocity of the gas phase at the axial position considered. The particle behaviour tends to that of the gas phase downstream of the axial location where the characteristic time of the particles becomes lower than that of the jet. At $x = 20D$, we can observe a good correspondence between the 10–15 and 20–25 μm particle size-classes and the fluid radial profiles. For the 30–35 and the 40–45 μm particles, a mean relative velocity subsists between the phases. At $x = 30D$, this relative velocity is only observed for 40–45 μm particles.

3.3. Distribution of the particle fluctuating velocity

The axial evolution of the streamwise fluctuating velocity of the continuous and dispersed phase are presented in figure 8. The profiles are normalised by the mean axial velocity of the continuous phase at the exit of the tube. After a phase of flow organisation, the particle fluctuating velocity reaches a maximum and then decreases as the gas phase component. We observe that the axial location of the maximum increases with the particle diameter and is, once more, correlated to the axial distance where the Stokes number becomes lower than one (reported in the figure).

Longitudinal evolutions of the radial velocity fluctuations normalised by the mean axial velocity of the gas phase at the exit of the tube are presented in figure 9. We detect great differences between the behaviour of the different size-classes. The radial fluctuating velocity of the 10–15 μm particles exhibits a maximum close to 10 jet diameters downstream and tends to that of the gas phase around 20 jet diameters. Once the influence of initial conditions become negligible, we see in figure 9 that no clear change in the behaviour of the bigger particles is detected to be correlated with the evolution of the Stokes number defined previously.

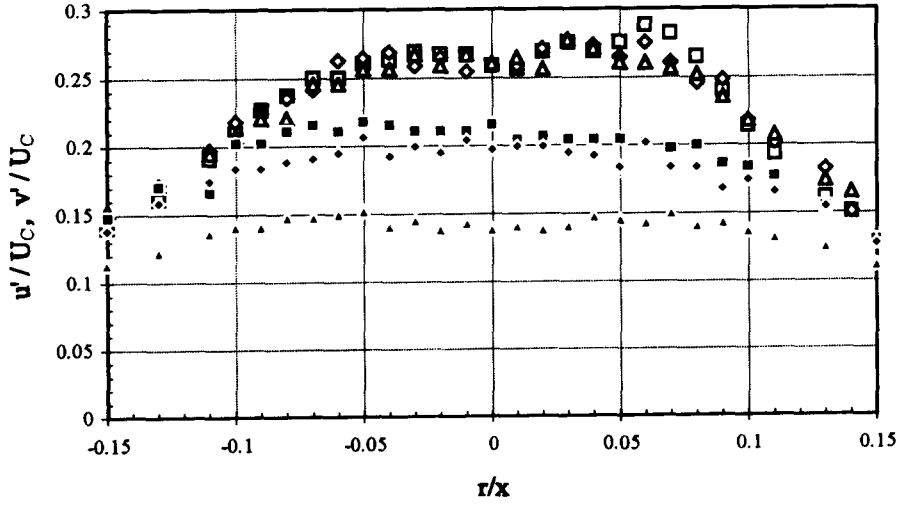

Figure 10. Streamwise and radial fluctuating fluid and particles velocity profiles at $x/D = 30$: □, $u'_f/U_{f,c}$; ◇, 10–15 μm $- u'_p/U_{p,c}$; △, 30–35 μm $- u'_p/U_{p,c}$; ■, $v'_f/U_{f,c}$; ◆, 10–15 μm $- v'_p/U_{p,c}$; ▲, 30–35 μm $- v'_p/U_{p,c}$.

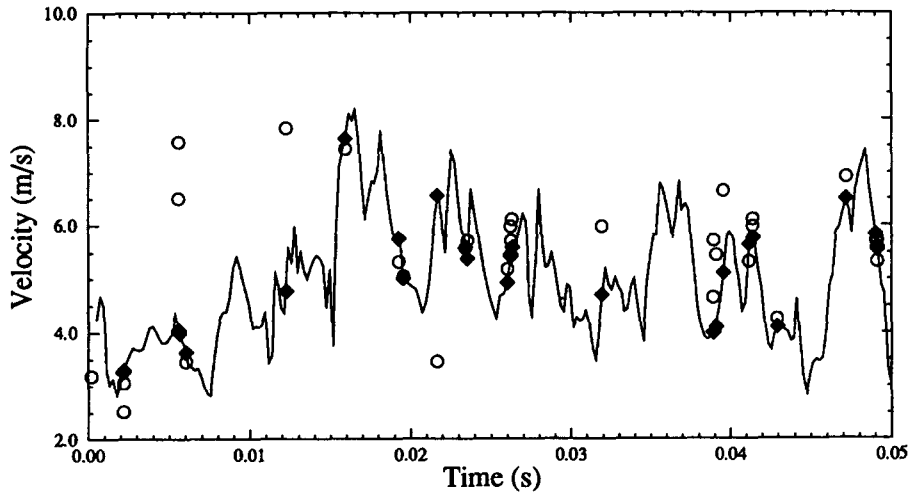

Figure 11. Velocity signal reconstructed at $x/D = 30$ on the jet axis; ——, reconstructed signal of the continuous phase; ◆, velocity of the fluid seen by the particles; ○, particle velocity.

The transverse profiles of the streamwise and radial fluctuating velocity at $30D$ normalised by the mean centreline velocity of each size-class are presented in figure 10. In order to facilitate the interpretation of the results we only present the two size-classes 10–15 and 30–35 μm in this figure. Previous studies (Fleckhaus *et al.* 1987; Hardalupas *et al.* 1989; Simonin 1991) have already shown the existence of a great anisotropy between the axial and radial velocity fluctuations of the particles in free shear flows. The ratio of the square fluctuating velocity components $\langle v^2 \rangle / \langle u^2 \rangle$ on the jet axis is here about 0.25 for the 30–35 μm particles whereas it is about 0.6 for the 10–15 μm particles and for the continuous phase. Following Simonin (1991) and Hishida *et al.* (1992) this difference arises from the production of particle turbulence by the mean particle velocity gradients. In a free shear flow, production of the streamwise fluctuating component is significantly higher and, for a negligible interparticle collision influence, the absence of redistribution from the longitudinal fluctuating component of the particles to the fluctuating velocities in the other directions explains the low level of the radial fluctuating velocity. Particle radial velocity fluctuations should be mostly controlled by the dragging by the fluid turbulent motion (Simonin 1991). Our results are in good agreement with these interpretations. The strong link between the mean longitudinal particle velocity field and the longitudinal fluctuating component is illustrated by the dimensional analysis presented before. Indeed, the Stokes number defined previously, well adapted to the description of the selective influence of the jet on the particles mean velocity field (see figure 5), is also well adapted to the particle longitudinal fluctuating component (see figures 8 and 10). Further evidence of these particular mechanisms and of the effect of particle inertia will be discussed in the last section of the paper.

4. MEASUREMENTS OF THE FLUID/PARTICLE CORRELATED MOTION

4.1. Methodology and validation

In the preceding section we have observed the selective influence of large eddy structures present in the jet on the velocity statistics of the particles. We can expect that the fluid–particle interactions lead to a non homogeneous instantaneous repartition of the particles across the flow. Evidently, we can't detect the large coherent structures in the jet far field by using single point measurements. However, the statistical signature (if any) of the turbulence on the spatial repartition of the particles could be detected if the undisturbed fluid velocity at the instantaneous spatial location of the particle was known. Moreover, it is now accepted that the fluid velocity "seen" by the particles is particularly important in modelling fluid–particle interactions in turbulent two-phase flows with Eulerian or Lagrangian approaches (Simonin *et al.* 1995). On a practical point of view, this velocity

corresponds to the instantaneous fluid velocity surrounding a particle whose diameter is ideally assumed much smaller than the smallest scales of turbulence.

We performed velocity and size measurements with a high density of flow tracers, seeded both in the jet and in the surrounding air, allowing an acquisition frequency larger than 20 times a frequency scale characteristic of the more energetic eddies. Following Hunt (1992), this frequency scale (F_i) is determined by the maximum shear rate: max $(\partial U_f/\partial r) \approx (U_{f,c}/0.1x)$. Only the velocity data from the tracers are kept in a first step and the time evolution of the fluid velocity is reconstructed by using the method proposed by Veynante & Candel (1988) based on the Shannon interpolation of the non regularly sampled turbulent signal of the gas phase. Knowing the arrival time of the particles in the measuring volume, it is then possible to know the fluid velocity seen by the particles defined previously. A sample of the reconstructed signal of the continuous phase, of the velocity of the fluid seen by the particles and of the particle velocity is given in figure 11. Measurements were carried out simultaneously on the two phases at four radial locations in the jet far field at 30 diameters from the exit of the tube. At $x/D = 30$, F_i is approximately equal to 150 Hz. We performed ensemble averaging of 10 000 samples for the fluid velocity and of more than 3000 samples for the velocity of the fluid seen by the particles of each size class. The expected statistical error bars for mean and standard deviation values are reported in the following graphs.

It is first important to assess precisely the accuracy of the method. In order to measure accurately instantaneous relative velocity, the reconstructed turbulent signal has at least to take into account the energetic turbulent structures of the flow. In order to validate the method with our high tracers density, we have tested first the convergence of the mean and standard deviation value of the fluctuating relative velocity between the fluid and the particles obtained by taking into account for the fluid velocity reconstruction all velocity measurements of the alcohol markers compared with one out of two, one out of five, one out of 10 and one out of 20. A convergence was observed when the number of velocity measurements conserved is greater than one out of five (Prévost *et al.* 1995). The energy density spectra of the reconstructed longitudinal velocity signal on the jet axis resampled at a constant frequency close to the mean acquisition frequency are compared in figure 12 for three different tests (all tracer measurements kept, one out of two and one out of five). We can notice a very good superposition of the spectra in the energy containing range. Moreover, we expect the smallest time scales to cause only small variations in the particle slip velocity. We therefore conclude that it is possible to compute with reasonable accuracy the velocity of the fluid seen by the particles.

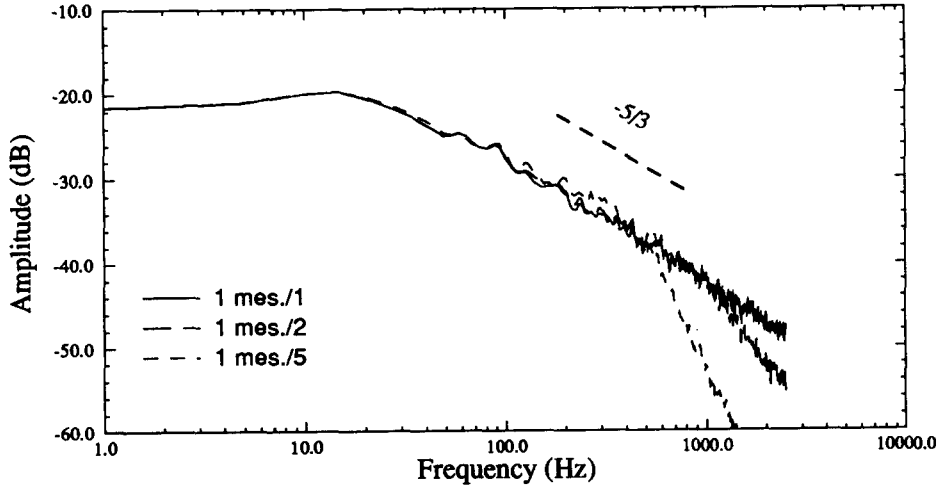

Figure 12. Energy density spectrum of the reconstructed longitudinal velocity signal on the jet axis as a function of the number of tracers measurements kept.

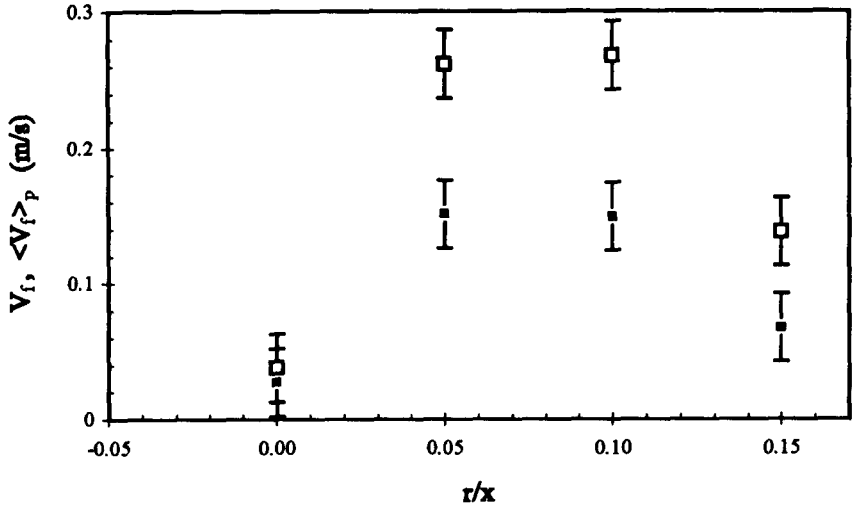

Figure 13. Mean radial velocity of the fluid seen by the particles at $x/D = 30$ compared to the mean radial velocity of the fluid: □, $\langle V_f \rangle_p$; ■, V_f.

4.2. *Mean fluid velocity seen by the particles*

The mean radial velocity profile of the fluid is compared to the mean radial velocity seen by the particles in figure 13. No significant differences between size classes were detected (Prévost 1994) and all classes are averaged for clarity in figure 13. We see clearly that the mean radial velocity of the fluid seen by the particles is much larger (up to 80% locally) than the mean radial fluid velocity. This observation is a direct consequence of the greater probability of presence of the particles in high outward radial velocity part of the flow. As a matter of fact, reference work of Longmire & Eaton (1992), concerning preferential concentration in the near field of a forced air jet showed that responsive particles become clustered in the saddle regions downstream of the deterministic vortex rings and are propelled away from the jet axis by outward moving flow in these regions. Such a description is expected to be valid, though less pronounced, in the far field turbulence. To complete this analysis, we have reported in figure 14 the radial evolution of the probability $P(V > 0)$ for particles to have an outward radial velocity at 30 jet diameters. This graph is based on measurements presented in section 3. On the axis of the jet, it shows the equiprobability for the particles to travel in either direction. Off-axis, the probability becomes greater for the

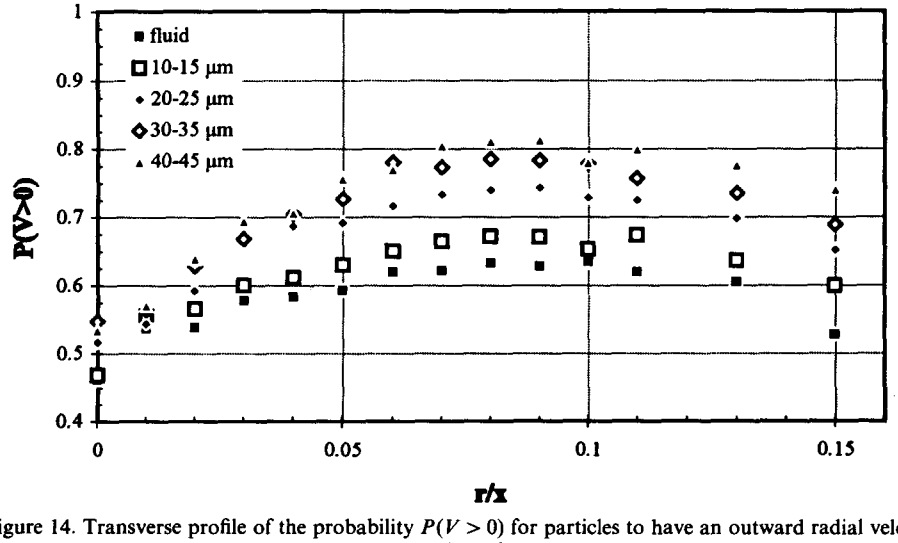

Figure 14. Transverse profile of the probability $P(V > 0)$ for particles to have an outward radial velocity at $x/D = 30$.

particles than for the markers of the continuous phase and tends to increase with the increase in the particle diameter. This observation complements the picture and shows the outward radial movement of the particles propelled away from the jet axis.

Contrary to mean radial velocities, no significant differences are found between the mean streamwise velocity of the fluid compared to the mean streamwise velocity of the fluid seen by the 10–15 μm (St(30D) $\approx$ 0.04); 20–25 μm (St(30D) $\approx$ 0.14) and 30–35 μm (St(30D) $\approx$ 0.3) particles not represented here. Only the mean streamwise velocity seen by the 40–45 μm (St(30D) $\approx$ 0.5) particles is significantly lower than the fluid velocity near the jet axis with $\langle U_{f,c}\rangle_p/U_{f,c} = 0.94$. This difference could also be in "statistical" agreement with near field measurements in forced air jet. Indeed, a simple potential flow computation shows that regions where particles are clustered downstream of the deterministic vortex rings are decelerating regions where the longitudinal velocity is lower than the mean velocity. More measurements would however be necessary to clarify this point.

The prediction of the mean relative velocity seen by the particles is important in Eulerian statistical approaches in order to predict accurately the mean interfacial transfers of momentum (Simonin 1991). A "drifting" velocity $V_{d,i}$ is introduced by Simonin with:

$$V_{d,i} = (\langle U_{p,i}\rangle_p - \langle U_{f,i}\rangle_f) - \langle U_{p,i} - U_{f,i}\rangle_p = \langle U_{f,i}\rangle_p - \langle U_{f,i}\rangle_f = \langle u_{f,i}\rangle_p.$$

The index i denotes here only the "i" direction, and u_f is the fluctuating fluid velocity with $\langle u_{f,i}\rangle_f = 0$. Figure 13 shows that V_d is a non negligible positive term in the radial direction. A negative value of V_d is detected in the longitudinal direction near the jet axis. Deutsch and Simonin (1991) derived a semi empirical model to predict V_d in homogeneous flows based on a gradient hypothesis. This approach was extended in non-homogeneous flows showing that V_d has to account for the influence of the mean fluid velocity shear and of the "turbulophoresis" mechanism induced by the difference between fluid and fluid–particle turbulent stresses (Simonin *et al.* 1993).

4.3. *Fluid–particle velocity correlation—discussion*

The fluid turbulent Reynolds stresses seen by the particles $\langle u_f u_f\rangle_p$ and $\langle v_f v_f\rangle_p$ were found in Prévost (1994) to lie very close to the fluid turbulent Reynolds stresses $\langle u_f u_f\rangle_f$ and $\langle v_f v_f\rangle_f$, respectively. No statistical preference is induced as far as fluid longitudinal and transverse Reynolds stresses are concerned.

The fluid–particle correlations $\langle u_f u_p\rangle_p$ and $\langle v_f v_p\rangle_p$ were derived from our measurements in order to give further insight into the flow physics and to validate some new approaches for the two fluid modelling of the particle fluctuating motion. Simonin (1991) has shown that solving separate transport equations for the components of the kinetic stress tensor of the particles and for the fluid–particle velocity covariance is necessary to predict accurately the high anisotropy level of the particle kinetic stress tensor in dilute shear flows.

The particle kinetic stress equation for dilute discrete solid particles suspended in a turbulent flow can be found in Simonin *et al.* (1995). In a stationary axisymmetric particle laden jet, equations for $\langle u_p u_p\rangle_p$ and $\langle v_p v_p\rangle_p$ read:

$$U_p\frac{\partial\langle u_p u_p\rangle_p}{\partial x} + V_p\frac{\partial\langle u_p u_p\rangle_p}{\partial r} = -2\left(\langle u_p u_p\rangle_p\frac{\partial U_p}{\partial x} + \langle u_p v_p\rangle_p\frac{\partial U_p}{\partial r}\right) - \frac{1}{\alpha_p}\left(\frac{\partial\alpha_p\langle u_p u_p u_p\rangle_p}{\partial x} + \frac{\partial r\alpha_p\langle u_p u_p v_p\rangle_p}{r\partial r}\right) - \frac{2}{\tau_p^f}(\langle u_p u_p\rangle_p - \langle u_f u_p\rangle_p) \quad [4]$$

$$U_p\frac{\partial\langle v_p v_p\rangle_p}{\partial x} + V_p\frac{\partial\langle v_p v_p\rangle_p}{\partial r} = -2\left(\langle u_p v_p\rangle_p\frac{\partial V_p}{\partial x} + \langle v_p v_p\rangle_p\frac{\partial V_p}{\partial r}\right) - \frac{1}{\alpha_p}\left(\frac{\partial\alpha_p\langle u_p v_p v_p\rangle_p}{\partial x} + \frac{\partial r\alpha_p\langle v_p v_p v_p\rangle_p}{r\partial r} - 2\frac{\alpha_p\langle v_p w_p w_p\rangle_p}{r}\right) - \frac{2}{\tau_p^f}(\langle v_p v_p\rangle_p - \langle v_f v_p\rangle_p) \quad [5]$$

where α_p is the particle volumetric fraction. τ_p^f, the mean particle relaxation time, is the Stokes characteristic time τ_p introduced previously but corrected for the nonlinear dependence of the drag coefficient upon the particle Reynolds number.

The first term on the right-hand side of [4] and [5] represents production from the particle mean velocity gradient. The second term is the transport of kinetic stress by the particle velocity fluctuations. The third term is an approximate form of the turbulent momentum transfer rate from the fluid turbulent motion. The first part of this contribution, proportional to the particle kinetic stress $\langle u_p u_p \rangle_p$ and $\langle v_p v_p \rangle_p$, respectively, is a sink term due to the drag force. Conversely, the second part of this contribution, proportional to the fluid–particle correlation $\langle u_f u_p \rangle_p$ and $\langle v_f v_p \rangle_p$, respectively, is a source term representing the dragging of the particle by the fluid turbulence (Simonin *et al.* 1995).

Using the classical boundary layer assumption (Tennekes & Lumley 1972), longitudinal diffusion and production terms can be neglected in [5]. Moreover, figures 9 and 10 show clearly that, once the influence of the initial conditions is negligible, v_p statistics are quasi uniform throughout the jet except for the smaller particle size class 10–15 μm. Equation [5] is expected to be significantly simplified at 30 jet diameters and reads:

$$\langle v_p v_p \rangle_p \approx \langle v_f v_p \rangle_p. \qquad [6]$$

The streamwise kinetic stress [4] is not so easily simplified as mean and fluctuating transport terms may play a significant role especially near the jet axis. In the limit of fluid particles, recent measurements of Panchapakesan & Lumley (1993) and Hussein *et al.* (1994) show that the shear production of $\langle u_f^2 \rangle_f$ is dominant about $r/x = 0.06$. On the jet axis, strain production, mean advection and turbulent diffusion of $\langle u_f^2 \rangle_f$ are comparable source terms. All contributions decrease when one moves outward from $r/x = 0.06$ and are very weak at $r/x = 0.15$. For glass particles and in the high shear region of the jet, [4] leads to the following approximate relation (Simonin 1995) between the dominant production term and the interphase momentum transfer rate:

$$\langle u_p u_p \rangle_p \approx \langle u_f u_p \rangle_p - \tau_p^f \langle u_p v_p \rangle_p \frac{\partial U_p}{\partial r}. \qquad [7]$$

Relation [7] shows that the streamwise particle velocity variance $\langle u_p u_p \rangle_p$ is expected to be significantly higher than the corresponding fluid–particle velocity correlation.

The measured quantities at $x/D = 30$ for the largest particle class are shown in figure 15. Measurements are in good agreement with the above modelling approach. The radial kinetic stress lie close to the radial fluid–particle velocity correlation. The transverse particle velocity component, controlled by the local dragging by the fluid turbulence [6] should therefore be predicted with reasonable accuracy by Tchen's theory (Simonin 1991). This point will be addressed below. On the other hand, $\langle u_p u_p \rangle_p$ is everywhere greater than $\langle u_f u_p \rangle_p$. The difference is maximum near the jet axis and in the high shear region. It then decreases sharply with increasing r/x and is negligible

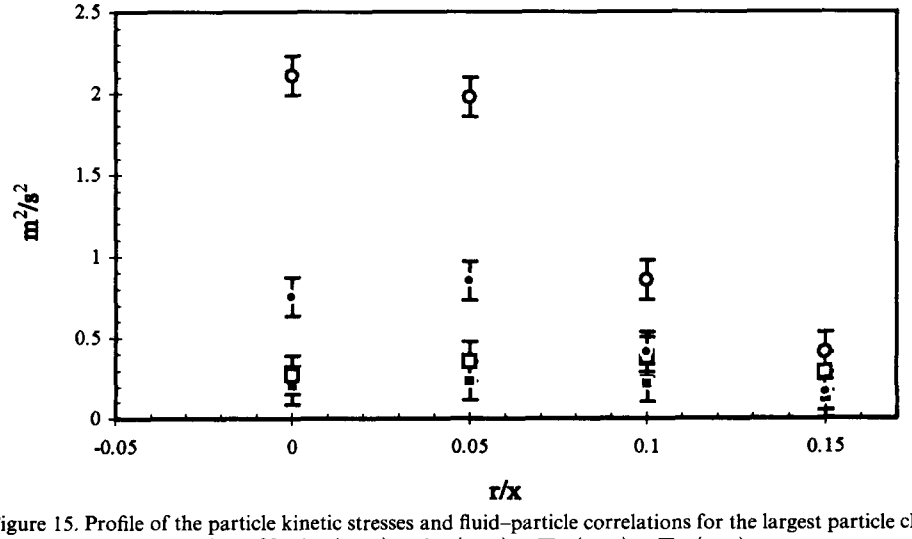

Figure 15. Profile of the particle kinetic stresses and fluid–particle correlations for the largest particle class at $x/D = 30$: ○, $\langle u_p u_p \rangle_p$; ●, $\langle u_f u_p \rangle_p$; □, $\langle v_p v_p \rangle_p$; ■, $\langle v_f v_p \rangle_p$.

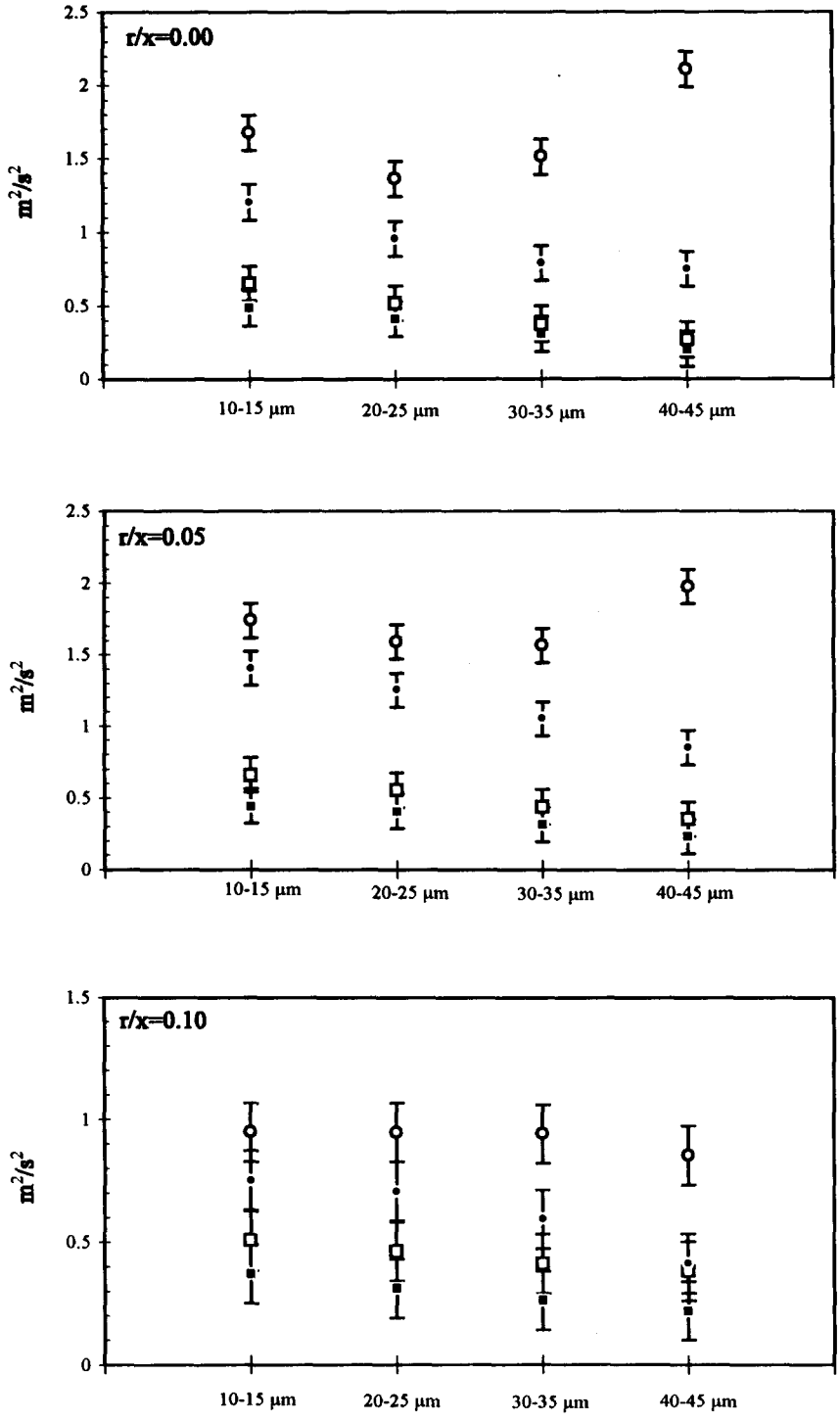

Figure 16. Influence of the particle diameter on the particle kinetic stresses and fluid–particle correlations at $x/D = 30$ and $r/x = 0.00$, 0.05 and 0.10: ○, $\langle u_p u_p \rangle_p$; ●, $\langle u_f u_p \rangle_p$; □, $\langle v_p v_p \rangle_p$; ■, $\langle v_f v_p \rangle_p$.

at $r/x = 0.15$. These observations stress the important role of production, advection and turbulent diffusion terms in fixing the level of $\langle u_p u_p \rangle_p$ in the jet.

It was observed in section 3 that a noticeable effect of particle inertia is to increase the degree of anisotropy of the particle fluctuating motion with respect to the fluid one. Figure 16 shows the effect of inertia on quantities $\langle u_p u_p \rangle_p$, $\langle u_f u_p \rangle_p$, $\langle v_p v_p \rangle_p$ and $\langle v_f v_p \rangle_p$ at $r/x = 0.00$, 0.05 and 0.10.

Table 1. Time scale ratios computed from the transverse particle kinetic stress measurements in the framework of Tchen theory (jet axis; $x/D = 30$)

d_p (μm)	10–15	20–25	30–35	40–45
η_r	2.5	1.3	0.7	0.4
τ_j/τ_p^t	8.7	5.2	4.7	4.5
τ_e/τ_p^t	2.4	1.4	1.3	1.3

$\langle u_f u_p \rangle_p$ and $\langle v_f v_p \rangle_p$, the longitudinal and radial dragging by the fluid turbulence, decrease with increasing particle relaxation time compared to the fluid turbulence integral time scale. The transverse kinetic stress therefore decreases simultaneously. In contrast, the difference between $\langle u_f u_p \rangle_p$ and $\langle u_p u_p \rangle_p$ increases and the streamwise component eventually grows for the bigger particle size class. In the high shear region of the jet, by $r/x = 0.05$, this evolution is well predicted by simplified equation [7]. In the present case, the lateral particle mean velocity gradient is approximately independent of the particle size at $x/D = 30$ (see figure 7). The particles shear stress component was unfortunately not measured in this study but is expected to decrease with increasing particle size (Fleckhaus *et al.* 1987). The increase in the particle relaxation time thus largely compensates for the expected decrease in $\langle u_p v_p \rangle_p$. Figure 16 shows that the relative increase in $\langle u_p u_p \rangle_p$ with particle diameter is also important on the jet axis and less pronounced at $r/x = 0.10$.

Predictions of the transverse kinetic stress in the framework of Tchen theory (Hinze 1959) lead to the following relation for solid particles ($\rho_p \gg \rho_f$):

$$\langle v_p v_p \rangle_p = \langle v_f v_f \rangle_p \frac{\eta_r}{1+\eta_r} \quad \text{where} \quad \eta_r = \frac{\tau_p^t}{\tau_p^f}. \qquad [8]$$

τ_p^t is the time scale of the fluid turbulent motion seen by the particles. η_r and τ_p^t were deduced from our measurements and are reported in table 1 for the different particle size classes. τ_p^t is compared to the "structural" eddy time scale introduced previously $\tau_j = 0.1x/u_f'$ which represents the time scale of the large eddies that span the whole jet flow. τ_p^t is also compared with the time scale τ_e of the more local eddy motion containing most of the turbulent energy (Hunt 1992). τ_e is classically determined by $\tau_e \approx (0.1x/U_{f,c})$.

While η_r decreases significantly with increasing particle relaxation time, we see that the ratio τ_j/τ_p^t and τ_e/τ_p^t is roughly independent of the diameter of the particle size class. Moreover, the time scale of the fluid turbulent motion seen by the particles is found to scale with the Eulerian time scale of the more energetic eddies τ_e. The exact relation between τ_e and τ_f^t, the Lagrangian integral time scale of the fluid turbulence, is unknown here. However, this scaling, quasi independent of the size class of the particles, provides a further signature of the dragging of the particles by the fluid turbulence which controls the transverse kinetic stresses of the particles.

5. CONCLUSION

Some typical features of fluid–particle correlated motion in the far field of an axisymmetrical polydispersed particle laden tube jet were presented in this paper. Measurements were obtained by using a phase Doppler anemometer allowing size and velocity measurements. The statistical properties of four particle size classes were displayed in order to cover a wide range of particle relaxation times.

A Stokes number based on a large eddy time scale was defined in section 3. A particular property of the jet flow is that the Stokes number decreases significantly as we move downstream. It was shown that this Stokes number is an appropriate parameter to describe the selective influence of the jet flow on the particle longitudinal mean velocity field. The measurements of the particle longitudinal and radial kinetic stresses illustrate clearly the strong link between the longitudinal fluctuating component and the mean longitudinal particle velocity field. The noticeable anisotropy between axial and radial fluctuating velocity of the particles is found to increase with increasing particle relaxation time scale.

A method was proposed and validated in order to determine statistics of the fluid velocity seen by the particles. These quantities are particularly important in understanding fluid–particle

interactions in turbulent two-phase flows. This method was applied in the jet far field at 30 diameters from the jet exit. The ejection of solid particles in high outward velocity regions is well detected: the mean radial velocity of the fluid seen by the particles is locally 80% greater than the mean radial velocity of the fluid. Results concerning mean fluid velocity seen by the particles are therefore in "statistical" agreement with previous experimental or numerical results obtained in a jet near field with well defined and identified coherent structures.

Finally, the behaviour of the particle longitudinal and radial kinetic stresses was studied in the frame of the Eulerian approach developed by Simonin (1991). The measured radial kinetic stress is found to lie very close to the measured radial fluid–particle correlation. Both terms are shown to decrease significantly with increasing particle relaxation time scale compared to the fluid turbulence integral time scale. On the contrary, the longitudinal kinetic stress is significantly greater than the measured longitudinal fluid–particle correlation. Moreover, the difference between these terms increases with particle relaxation time scale.

Following Simonin *et al.* (1995), the equations governing the particle kinetic stresses were written. Our measurements are in agreement with the predicted trends and show the important contribution of production, advection and turbulent diffusion terms in fixing the level of the longitudinal particle kinetic stress in the jet. In the high shear region of the jet, the production of longitudinal kinetic stress by the mean particle velocity gradient is the main contributor to the difference between $\langle u_p u_p \rangle_p$ and $\langle u_f u_p \rangle_p$ and the increase of this difference with increasing particle relaxation time scale is explained. On the other hand, it appears clear that the radial kinetic stress is mainly controlled by dragging from fluid turbulence. Tchen's theory is thus found to provide a physically consistent scaling of the time scale of the fluid turbulent motion seen by the particles which is quasi independent of the chosen size class.

Measurements of the fluid statistics seen by the particles, in particular fluid–particle correlations, are believed to provide a rich understanding of the fluid–particle interactions in a jet far field. Such quantities have been obtained previously from numerical simulations in basic turbulent flows. The results of the experiments described here are especially valuable for testing correlation models and other heuristic models of complex turbulent flows.

Acknowledgements—We wish to thank Dr O. Simonin and Prof. E. K. Longmire for their helpful comments about this work. We have benefited greatly from the technical support of G. Couteau, J. F. Alquier and Y. Aubry (Onera-Cert Dero).

REFERENCES

Berlemont, A., Desjonqueres, P. & Gouesbet, G. 1990 Particle Lagrangian simulation in turbulent flows. *Int. J. Multiphase Flow* **16,** 19–34.

Deutch, E. & Simonin, O. 1991 Large eddy simulation applied to the motion of particles in stationary homogeneous fluid turbulence. *Turbulence Modification in Multiphase Flows* **110,** 35–42.

Dimotakis, P. E., Miake-Lye, R. C. & Papantoniou, D. A. 1983 Structure and dynamics of round turbulent jets. *Phys. Fluids* **26,** 3185–3192.

Eaton, J. K. & Fessler, J. R. 1994 Preferential concentration of particles by turbulence. *Int. J. Multiphase Flow* **20,** 169–209.

Elgobashi, S. E. & Abou-Arab, T. W. 1983 A two-equation turbulence model for two-phase flows. *Phys. Fluids* **26,** 931–938.

Fleckhaus, D., Hishida, K. & Maeda, M. 1987 Effects of laden solid particles on the turbulent flow structure of a round free jet. *Exp. Fluids* **5,** 323–333.

Hardalupas, Y., Taylor, A. M. K. P. & Whitelaw, J. H. 1989 Velocity and particle-flux characteristics of turbulent particle-laden jets. *Proc. R. Soc. Lond.* 31–78.

Heitor, M. V. & Moreira, A. L. N. 1994 Experiments on polydisperse two-phase turbulent jets. *Proc. ICLASS-94,* Rouen, pp. 930–937.

Hinze, J. O. 1959 *Turbulence.* McGraw-Hill, New York.

Hishada, K., Ando, A. & Maeda, M. 1992 Experiments on particle dispersion in a turbulent mixing layer. *Int. J. Multiphase Flow* **18,** 181–194.

Hunt, J. C. R. 1992 Developments in computational modelling of turbulent flows. In *Proceedings of the ERCOFTAC Workshop on Numerical Simulation of Unsteady Flows* (Edited by O. Pirroneau *et al.*). Cambridge University Press, Cambridge.

Hussein, H. J., Capp, S. C. & George, W. K. 1994 Velocity measurements in a high-Reynolds-number, momentum conserving, axisymmetric, turbulent jet. *J. Fluid Mech.* **258,** 31–75.

Ishima, T., Hishida, K. & Maeda, M. 1993 Effects of particle residence time on particle dispersion in a plane mixing layer. *J. Fluids Engng* **115,** 751–759.

Lee, K. B. & Chung, M. K. 1987 Refinement of the mixing-length model for prediction of gas–particle flow in a pipe. *Int. J. Multiphase Flow* **13,** 275–282.

Longmire, E. K. & Eaton, J. K. 1992 Structure of a particle-laden round jet. *J. Fluid Mech.* **236,** 217–257.

Longmire, E. K. & Eaton, J. K. 1994 Active open-loop control of particle dispersion in round jets. *AIAA J.* **32,** 555–563.

Modarress, D., Tan, H. & Elghobashi, S. 1984 Two component LDA measurement in a two-phase turbulent jet. *AIAA J.* **22,** 624–630.

Mostafa, A. A., Mongia, H. C., McDonell, V. G. & Samuelsen, G. S. 1989 Evolution of particle-laden jet flows: a theoretical and experimental study. *AIAA J.* **27,** 167–183.

Panchapakesan, N. R. & Lumley, J. L. 1993 Turbulence measurements in axisymmetric jets of air and helium. Part 1. Air jet. *J. Fluid Mech.* **246,** 197–223.

Petrie, H. L., Samimy, M. & Addy, A. L. 1988 Laser Doppler velocity bias in separated turbulent flows. *Exp. Fluids* **6,** 80–88.

Picart, A., Berlemont, A. & Gouesbet, G. 1986 Modelling and predicting turbulence fields and the dispersion of discrete particles transported by turbulent flows. *Int. J. Multiphase Flow* **12,** 237–261.

Prévost, F. 1994 Comportement de particules solides polydispersées dans un jet d'air turbulent, *Ph.D. Thesis* I.N.P. Toulouse.

Prévost, F., Borée, J. & Charnay, G. 1995 Experimental analysis of an axisymmetric turbulent air jet laden with polydispersed solid particles. In *Proc. Int. Symp. on Two-phase Flow Modelling and Experimentation*, Rome.

Prévost, F., Borée, J., Nuglisch, H.-J. & Charnay, G. 1994 Characterisation of a polydispersed particle-laden jet using a phase Doppler anemometer. In *Proc. ICLASS-94*, Rouen, pp. 938–945.

Simonin, O. 1991 Prediction of the dispersed phase turbulence in particle-laden jets. In *Proc. 4th Int. Symp. on Gas–Solid Flows*, ASME FED, Vol. 121, 197–206.

Simonin, O. 1995 Private communication.

Simonin, O., Deutch, E. & Boivin, M. 1995 Large eddy simulation and second moment closure model of particle fluctuating motion in two-phase turbulent shear flows. In *Selected Papers from the Ninth Int. Symp. on Turbulent Shear Flows* (Edited by F. Durst, N. Kasagi, B. E. Launder, F. W. Schmidt, K. Suzuki & J. H. Whitelaw). Springer, Berlin, pp. 85–115.

Simonin, O., Deutch, E. & Minier, J. P. 1993 Eulerian prediction of the fluid/particle correlated motion in turbulent two-phase flows. *Appl. Sci. Res.* **51,** 275–283.

Tchen, C. M. 1947 Ph.D. thesis, University of Delft, the Hague.

Tennekes, H. & Lumley, J. L. 1972 *A First Course in Turbulence.* The M.I.T. Press, Cambridge.

Tso, J. & Hussain, A. K. M. F. 1989 Organised motion in excited free shear flows. *J. Fluid Mech.* **203,** 425–448.

Tsuji, Y., Morikawa, Y., Tanaka, T., Karimine, K. & Nishida, S. 1988 Measurement of an axisymmetric jet laden with coarse particles. *Int. J. Multiphase Flow* **14,** 565–574.

Veynante, D. & Candel, S. M. 1988 Application of non linear spectral analysis and signal reconstruction to laser Doppler velocimetry. *Exp. Fluids* **6,** 534–540.

Zoltani, C. K. & Bicen, A. F. 1991 Visualisation of fan-spreading in two-phase jet flows. *Exp. Fluids* **10,** 299–300.